Solar Energy 138 (2016) 67–76

Contents lists available at ScienceDirect

Solar Energy

journal homepage: www.elsevier.com/locate/solener

Comparative study between two novel sensorless and sensor based dual-axis solar trackers

Hassan Fathabadi

School of Electrical and Computer Engineering, National Technical University of Athens (NTUA), Athens, Greece

ARTICLE INFO

Article history:
Received 21 February 2016
Received in revised form 30 August 2016
Accepted 13 September 2016

Keywords:
Solar energy conversion
Sensor based solar tracker
Sensorless solar tracker

ABSTRACT

Two novel solar trackers are designed and constructed. The two trackers are novel because the first one that is a sensorless dual-axis solar tracker has a tracking error of only 0.43° which is less than that of the other sensorless and even most sensor based solar trackers reported in the literature, and the tracking error of the second tracker that is a sensor based dual-axis solar tracker is at most 0.14° which is explicitly less than that of the state-of-the-art sensor based solar trackers. The other contribution of this work is that the performances of the two trackers are compared to each other. On the one hand, it is experimentally verified that applying the sensor based solar tracker to a PV panel fixed to the sun's noon position increases the average daily captured solar energy about 27.7%, 32.5%, 37.3%, 42.7% and 35.22% respectively in winter, spring, autumn, summer and during one year. For the sensorless tracker, these factors are less, so that, they are respectively 19.1%, 22.4%, 26.1%, 30.2% and 24.59%. On the other hand, the sensor based solar tracker is more complicated and expensive because it needs one sensor equipped with a radiance limiting tube and extra mechanical components.

1. Introduction

A PV module/panel/array or solar concentrator converts solar energy into electric or thermal energy (Fathabadi, 2016). To extract the maximum output power from a PV module or solar concentrator, a solar tracker can be used to track the sun direction where sunbeam is perpendicular to the face of the PV module or solar concentrator, and the maximum value of solar energy is captured (Eldin et al., 2015; Nenciu and Vaireanu, 2014). For PV systems, previous researches showed that about 20–50% more solar energy can be captured depending on the geographic location by adding a solar tracker to a PV system (Quesada et al., 2015). Solar trackers are divided into two types: single-axis and dual-axis (Sallaberry et al., 2015). The sole axis of a single-axis solar tracker is aligned along the local north meridian, it has only one freedom degree, so it can only track the sun in one direction which is the daily path of the sun (Chong and Wong, 2009). A dual-axis solar tracker has two freedom degrees, so it can track the sun path in two directions which are daily and seasonal motions of the sun (Barker et al., 2013). A single-axis solar tracking system increases the daily output power of the PV module up to about 20% compared to a fixed PV module (Al-Mohammad, 2004). It is clear that a dual-axis solar tracking system is more accurate to track the sun direction compared to a single-axis type (Eke and Senturk, 2012). The output power of a PV module can be enhanced up to about 33% compared to a fixed PV module by utilizing a dual-axis solar tracker (Roth et al., 2005), although the amount of the improvement factor depends on the local latitude and the patterns of direct and diffuse sunlight. Single- and dual-axis trackers are classified into two types: sensor based and sensorless solar trackers. A sensor based solar tracker acts as a closed loop system in which photo sensors are used to provide appropriate feedback signals for tracking the sun direction using a feedback control system (Zhang et al., 2013). For instance, a single-axis solar tracker which uses two light-dependent resistor (LDR) sensors to provide feedback signals to obtain the correct azimuth angle showing the daily path of the sun (Chin et al., 2011). In high accurate sensor based dual-axis solar trackers, the sensors equipped with radiance limiting tubes are carried and oriented by a separate dual-axis mechanical system to find the sun direction, and then, the correct angles of the sun position obtained by the sensors are used by the solar tracker to orient the PV module or solar concentrator face toward the sun (Cañadaa et al., 2007). Thus, two independent dual-axis mechanical systems are needed; one for carrying the sensors, and the other one for PV module or solar concentrator. It is clear that the reference points of the two mechanical systems should be identical. A parallel mechanical mechanism investigated by utilizing Grassmann line geometry was proposed in Wu et al. (2016). The design

E-mail address: h4477@hotmail.com

http://dx.doi.org/10.1016/j.solener.2016.09.009
0038-092X/

reduces the driving torque needed for rotating the solar mirror or PV panel mounted on a dual-axis solar tracker. If high accurate equipped sensors are used, the tracking error of a sensor based dual-axis solar tracker can be limited up to 0.15° (Yao et al., 2014). However, using cheap sensors without radiance limiting tubes or mounting them on the PV module or solar concentrator not only significantly increases the tracking error but also reduces the system robustness. For instance, a sensor based dual-axis solar tracker designed using a simple four-quadrant LDR sensor beside a cylinder all attached to the PV panel was reported in Wang and Lu (2013). The shadow of the cylinder on the four LDRs is used to provide two feedback signals; one for azimuth angle and the other one for altitude angle. A similar dual-axis solar tracker which uses the effect of shadow on four LDRs was proposed in Barsoum (2011). It is clear that the tracking error of these kinds of sensor based dual-axis solar trackers is even more than 1°. A sensorless dual-axis solar tracker acts as an open loop system, it uses the offline estimated data about the sun path in the sky obtained from different sun path charts or solar map equations (Duarte et al., 2011). For a high qualified sensorless dual-axis solar tracker, a tracking error of up to 0.45° is achievable (Tirmikci and Yavuz, 2015), and a new set of data is also needed by changing the geographical location of the PV module or solar concentrator. The implementation of a small-sized sensorless dual-axis solar tracker which uses the azimuth and altitude angles provided by a database was reported in Syafii et al. (2015). Although, there is no report about the tracking error, a test performed for seven hours showed that about 26% more energy can be captured by utilizing the tracker compared to a flat-positioned PV module. A model-based simulation of an intelligent microprocessor-based standalone solar tracking system was studied to evaluate the impacts of environmental conditions on the simulated solar tracker (Chin, 2012). Based on two mathematical models; Evans and simplified type, a probabilistic model was presented to estimate the energy production of dual-axis solar trackers (Tina et al., 2012).

In this study, two novel dual-axis solar trackers are presented; the first one is sensorless while the second one is sensor based. The tracking errors of the two trackers are respectively 0.43° and 0.14° that are less than that of the state-of-the-art sensorless and sensor based solar trackers. The two solar trackers have been constructed, and are compared to each other and the state-of-the-art trackers from different viewpoints. The implementation of the proposed sensorless solar tracker is presented in detail in Section 2. Section 3 deals with the proposed sensor based solar tracker. The two solar trackers are compared to each other and the state-of-the-art trackers in Section 4, and the paper is concluded in Section 5.

2. Design and implementation of the proposed sensorless solar tracker

The schematic diagram of the PV system including the proposed sensorless solar tracker is shown in Fig. 1. The solar tracker consists of a controller, the stepper motor 1 which has been coupled to the altitude gear box, the stepper motor 2 which has been coupled to the azimuth gear box, the altitude gear box that rotates the PV module/panel in the vertical plane around the altitude axis, and the azimuth gear box which similarly rotates the PV module/panel in the horizon plane around the azimuth axis. The controller calculates the altitude and azimuth angles, and produces a set of appropriate control signals for the two stepper motors that will be explained in detail next. The declination angle is first calculated by the controller as (Duffie and Beckman, 2013):

$$\delta = \sin^{-1}\left(\sin(23.45^\circ)\sin\left(\frac{360}{365}(d-81)\right)\right) \quad (1)$$

where δ is the declination angle, and d is the day number of the year, so that, January 1 is taken into account as $d = 1$. The altitude angle denoted by α is then obtained as (Reda and Andreas, 2004):

$$\alpha = \sin^{-1}(\sin(\delta)\sin(\varphi) + \cos(\delta)\cos(\varphi)\cos(15^\circ(LST - 12))) \quad (2)$$

where φ is the latitude of the solar tracker location, and LST is the local solar time. After that, the azimuth angle denoted by β is found as:

$$\beta = \cos^{-1}\left(\frac{\sin(\delta)\cos(\varphi) - \cos(\delta)\sin(\varphi)\cos(15^\circ(LST-12))}{\cos(\alpha)}\right) \quad (3)$$

The azimuth angle is between 0° and 180° when the hour angle ($15^\circ(LST - 12)$) is negative (morning), and is between 180° and 360° when the hour angle is positive (afternoon).

2.1. Implementation of the sensorless solar tracking system

The structure of the PV system constructed to implement the proposed sensorless solar tracker is shown in detail in Fig. 2. It consists of a PV module, a DC/PWM converter, a controller, two stepper motor drivers, two stepper motors, and two gear boxes. To construct an accurate solar tracker, a set of electrical and mechanical components should be chosen, so that, a highly accurate rotation of the PV panel/module around the altitude and azimuth axes can be established. In this study, to provide a high-resolution rotation for the PV panel/module, so that, each step of the rotation being equal to only 0.12°, the components have been selected as below:

(A) **Stepper motors:** Two identical stepper motors with the step angle of 1.8° have been used; one for adjusting altitude angle, and the other one for adjusting azimuth angle.

(B) **Stepper motor drivers:** Two identical stepper motor drivers have been dedicated to the two stepper motors. Each driver supplies appropriate control signals and supply voltage to the associated stepper motor, so that, the stepper motor rotates according to the direction and the steps number requested by the controller.

(C) **DC/PWM converter:** The simple DC/PWM converter used in the constructed system is shown in Fig. 3. It consists of only one MOSFET switch S that switches with a constant switching period of $T_i = 1/f_i$, and a duty ratio of $D_S = t_{S-on}/T_i$, where f_i and t_{S-on} are the switching frequency and the switch S on-time, respectively. When S is turned on, the load current $I_L(t)$ flows through S and arrives to the load R_L. When S is turned off, $I_L(t)$ immediately reaches zero, so during t_{S-on}, the load current $I_L(t)$ is expressed as:

$$I_L(t) \approx \frac{V_{pv}}{R_{ds} + R_L} = I_B \quad (4)$$

where R_{ds} is the static drain to source on-resistance of the MOSFET switch S. In steady state, V_{pv} is approximately constant, and the voltage loss across the filter inductor L_{pv} is negligible, so the load current $I_L(t)$ can be considered as a constant current I_B during t_{S-on}. Thus, the load current $I_L(t)$ can be estimated as the PWM waveform shown in Fig. 4. The DC term (average) of the load current denoted by I_{L-DC} can be obtained as:

$$I_{L-DC} = D_S\frac{V_{pv}}{R_{ds} + R_L} \approx D_S I_B \quad (5)$$

It is deduced from Eq. (5) that the duty ratio D_S is a control signal which adjusts the DC load current to a specific level.

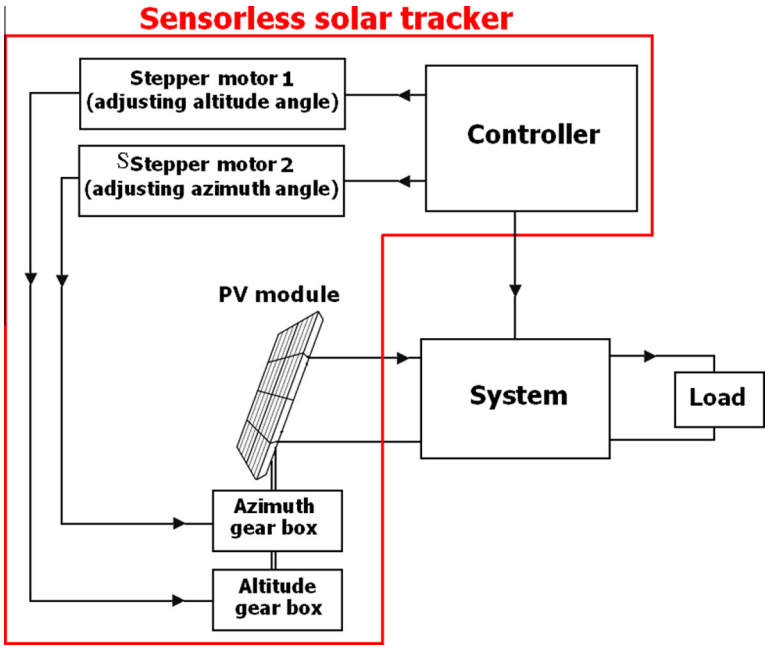

Fig. 1. Schematic diagram of the PV system including the proposed sensorless solar tracker.

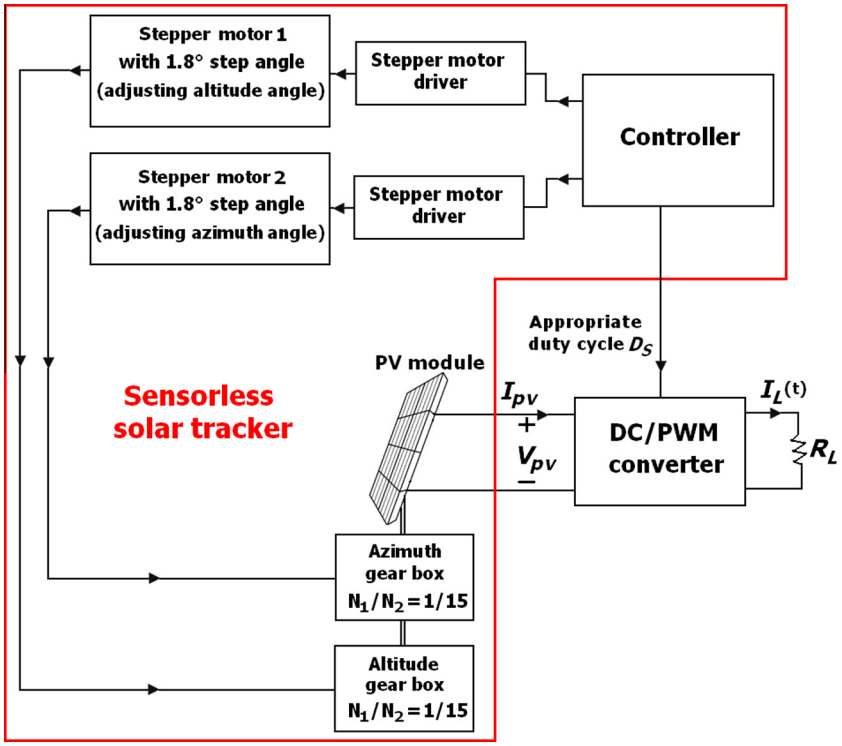

Fig. 2. Structure of the PV system constructed to implement the proposed sensorless solar tracker.

(D) **Controller:** The controller calculates the altitude and azimuth angles using Eqs. (1)–(3), and then produces the control signals which should be supplied to the two stepper motor drivers to rotate the two stepper motors in correct directions with the rotation angles calculated by the controller.

(E) **PV module:** One commercial PV module Suntech STP 300-24/Ve has been used in this study that its technical specifications under STC (standard test condition: Solar irradiance $G = 1000\ \mathrm{W\ m^{-2}}$, air mass (AM) 1.5 solar radiation spectrum, cell temperature $T = 25\ ^{\circ}\mathrm{C}$, and solar angle $\theta_z = 48.19^{\circ}$) extracted from the production datasheet are summarized in Table 1.

(F) **Mechanical components:** The mechanical components of the system are the two identical gear boxes shown in Fig. 2. The altitude gear box is used for rotating the PV module in the vertical plane around the altitude axis, and the azimuth gear box rotates the PV module in the horizon

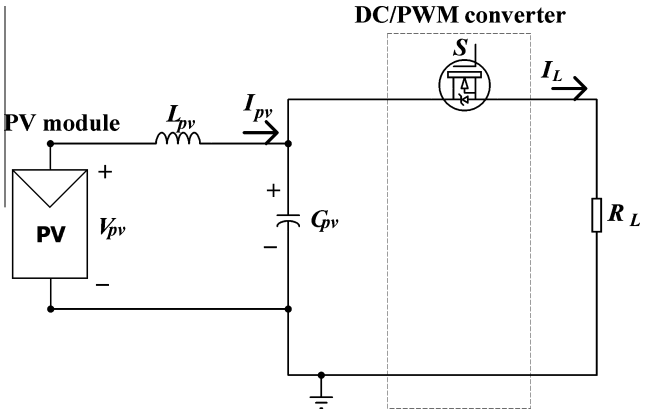

Fig. 3. Proposed simple DC/PWM converter.

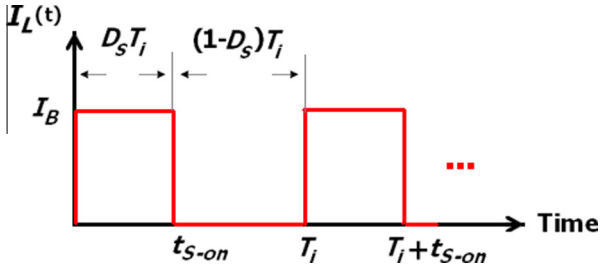

Fig. 4. Waveform of the load current $I_L(t)$.

Table 1
Parameters of the two constructed PV systems, and the specifications of the PV module STP 300-24/Ve used in the two PV systems.

PV module STP 300-24/Ve		DC/PWM converter	
Current at MPP I_{pv-mpp} (A)	8.36	f_i (kHz)	10
Voltage at MPP V_{pv-mpp} (V)	35.9	MOSFET switch S	IRF1407
Output power at MPP P_{pv-mpp} (W)	300	PV filter	
Short-circuit current I_{SC} (A)	8.83	C_{pv} (μF)	470
Open-circuit voltage V_{OC} (V)	44.5	L_{pv} (μH)	820
Stepper motor NEMA 23		Stepper motor driver AMIS-30543	

plane around the azimuth axis. Thus, the altitude gear box has been installed horizontally on the PV module axis while the azimuth gear box has been placed vertically as shown in Fig. 5(a) and (b). Each gear box consists of two gearwheels; one primary gearwheel, and one secondary gearwheel with the gear ratio of $N_1/N_2 = 1/15$. The advantages of utilizing these two gear boxes are:

- Each stepper motor has a step angle of 1.8°, and its dedicated gearbox has a gear ratio of 1/15, so each rotation step of the stepper motor (1.8°) is converted into a rotation step of 0.12° on the secondary shaft of the gearbox coupled to the PV module/panel. This provides a very small rotation step of only 0.12° for rotating the PV module/panel around the altitude and azimuth axes, and thus, significantly decreases the tracking error.
- Since the gear ratio is $N_1/N_2 = 1/15$, each gear box increases the holding torque of the associated stepper motor by a factor of 15. Thus, the driving torque on the secondary shaft of the gearbox used to rotate the PV module/panel significantly increases. For instance, each stepper motor used in this study has the holding torque of 9 kg-cm, so the driving torque is about 135 kg-cm which is great enough to move even heavy and large PV panels in practical applications.
- A combination of a gear box coupled to a stepper motor allows us not to use any brake system or torque reducer, and this not only significantly decreases the fabrication cost but also simplifies the solar tracker structure.
- Each gear box consists of only two very simple gearwheels as shown in Fig. 5(a) and (b), so in practice, there is not any cost or problem for maintaining them.

The assembled mechanical part of the solar tracker together with the PV module STP 300-24/Ve installed on it is shown in Fig. 5(c).

2.2. Sensorless solar tracker: Experimental results and performance evaluation

A PV system has been built to experimentally evaluate the performance of the proposed sensorless solar tracker. The electrical circuit of the PV system constructed to implement the sensorless solar tracker is shown in Fig. 6. The controller has been implemented using a microcontroller MC68HC11A8. The opto-diac S delivers a periodic switching pulse with the period of $T_i = 100$ μs ($f_i = 10$ kHz) and the duty ratio of D_S that is produced and adjusted by the microcontroller according to the user's command. Two stepper motor drivers AMIS-30543 have been used, one for driving the altitude stepper motor and another for driving the azimuth stepper motor. Each deriver has been connected to the microcontroller through the five wires, and receives five control signals from the controller. Two stepper motors NEMA 23 with holding torque of 9 kg-cm have been also used; one for adjusting the altitude angle α, and another for azimuth angle β. The microcontroller MC68HC11A8 has been programmed using C++ language to numerically solve Eqs. (1)–(3). In fact, in each step of the tracking process, it calculates the altitude and azimuth angles using Eqs. (1)–(3), and then produces the control signals which should be supplied to the two stepper motor drivers to rotate the two stepper motors in correct directions with the rotation angles calculated by the microcontroller. The above process repeats until the altitude and azimuth angles converge to the correct tracking angles α_T and β_T. In detail, when the next altitude/azimuth angle is more than the current amount, the microcontroller sets the DIR control signal to high (+5 V), and the NXT (STEP) control signal is supplied by an appropriate number of pulses from 0 V to +5 V. To obtain the number of the pulses which is needed, the microcontroller first subtracts the next amount of the angle from the current amount, and then divides the result by 0.12°. Similarly, when the next altitude/azimuth angle is less than the current amount, the DIR control signal is set low (0 V) by the microcontroller, and the number of the pulses is obtained by dividing the difference between the current and next amounts of the angle by 0.12°. Each stepper motor driver is also first enabled and configured by the microcontroller through the serial peripheral interface (SPI) pins consisting of DI (SPI data input), CS (SPI chip select), and CLK (SPI clock input). Thus, the microcontroller produces the ten control signals to be supplied to the two stepper motor drivers. The controller also produces an appropriate duty ratio D_S to be supplied to the DC/PWM converter based on the use's command to provide the output power level requested by the user. The technical specifications of the different parts of the constructed PV system are also summarized in Table 1.

The constructed solar tracking system was turned on. The actual altitude and azimuth angles of the sun position in the sky observed from the PV module situated in the geographic position

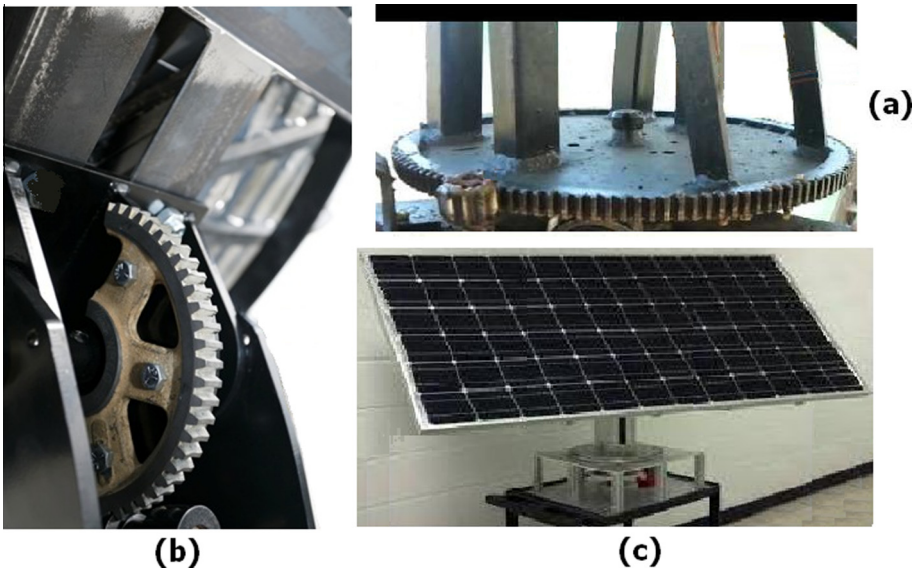

Fig. 5. Mechanical components of the constructed solar tracker: (a) Azimuth gear box and (b) altitude gear box and (c) whole of the assembled mechanical part together with the PV module STP 300-24/Ve installed on it.

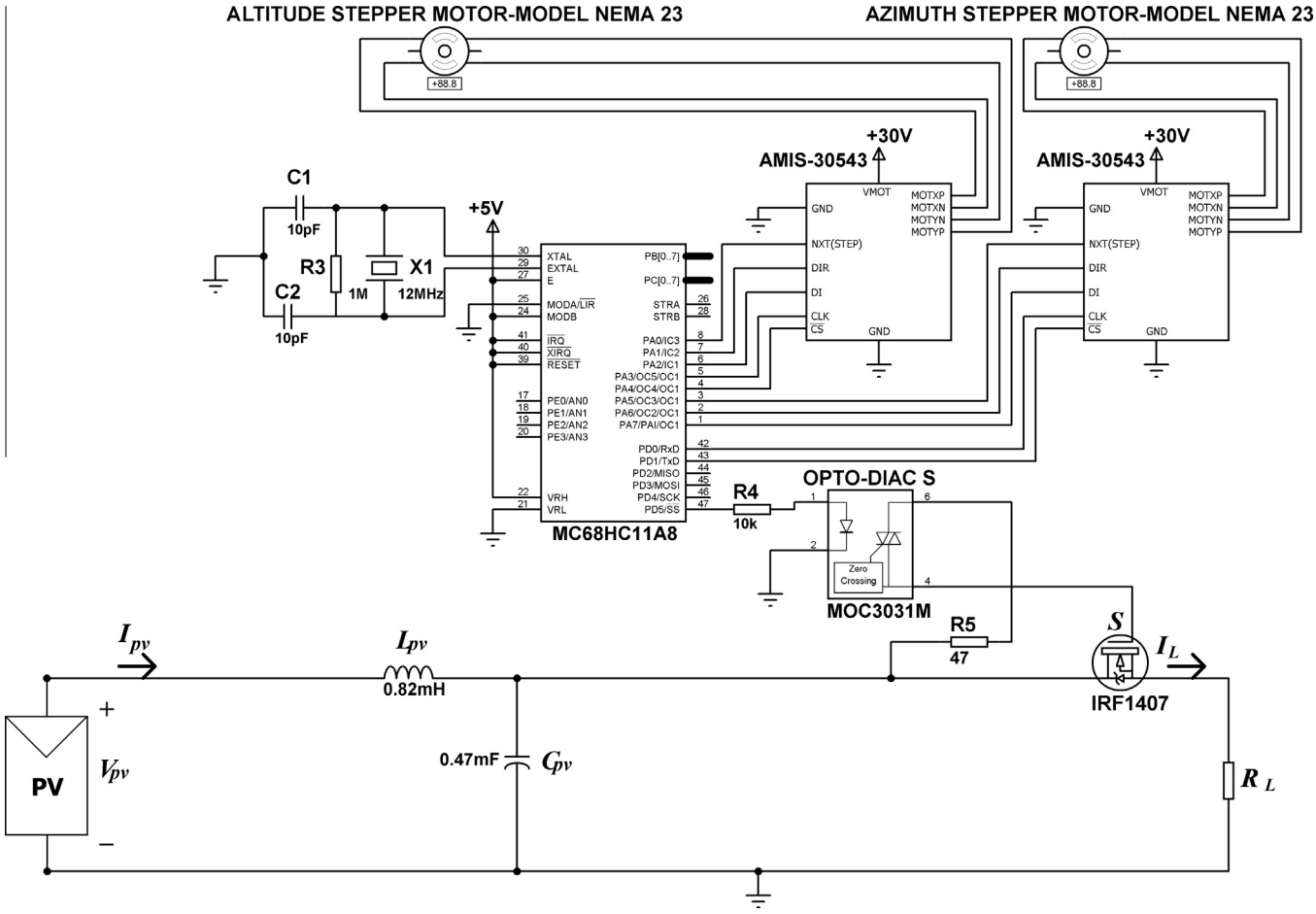

Fig. 6. Electrical circuit of the constructed PV system including the proposed sensorless solar tracker.

of (37.9667° N, 23.7167° E) were measured from hour to hour in daylight (6:00–21:00) on August 19, 2015 using two digital protractors with the accuracy of ±0.01°; one for measuring altitude angle and another for azimuth angle. Fig. 7(a) and (b) compare the actual values of the altitude and azimuth angles of the sun position to the altitude and azimuth angles tracked by the proposed sensorless solar tracker. The comparison shows that the maximum value of the tracking error is 0.43°, so the tracking error

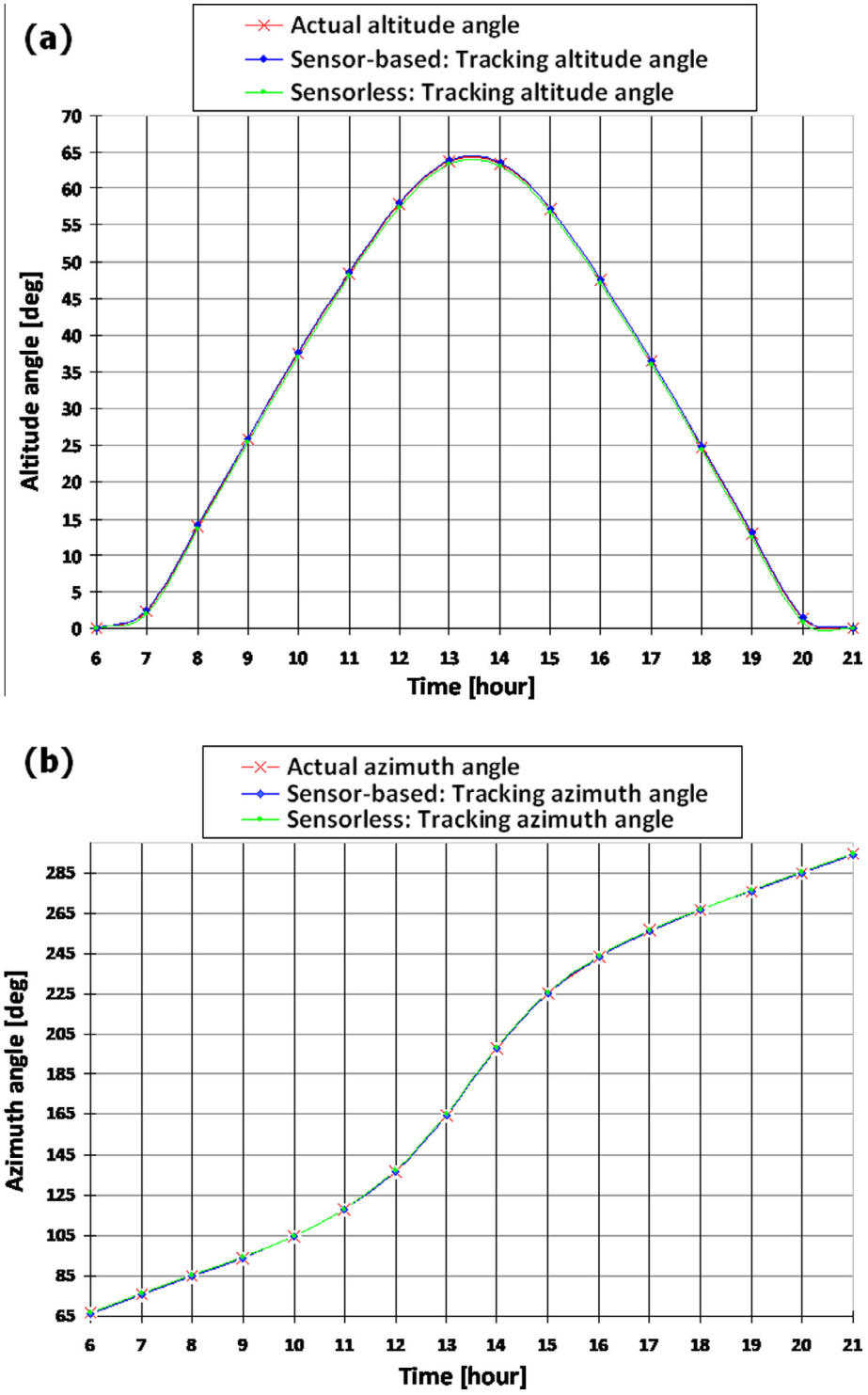

Fig. 7. Comparing between the actual altitude and azimuth angles measured from hour to hour in daylight (6:00–21:00) on August 19, 2015 and the angles tracked by the proposed sensorless and sensor based solar trackers.

of the proposed sensorless solar tracker is 0.43° in the azimuth and altitude angles.

In other experiments, the daily output powers of the PV module were measured from hour to hour in daylight on January 19, 2014 in winter and on August 19, 2015 in summer. Each measurement was performed twice; at the first time, it was measured when the implemented sensorless solar tracker was active (sensorless tracking mode). At the second time, it was measured when the solar tracker was off, and the PV module was fixed at the noon position of the sun (fixed mode). The daily output powers measured in winter and summer for both the sensorless tracking and fixed modes are shown in Fig. 8(a) and (b), respectively. It can be seen from Fig. 8(a) that in winter, the daily electric energies produced by the PV module on the fixed and sensorless tracking modes are respectively about 1.1422 kW h and 1.3599 kW h, and thus, the solar energy converted on the sensorless tracking mode is 19.1% more than that on the fixed mode. Similarly, Fig. 8(b) shows that the daily electric energies obtained on the fixed and

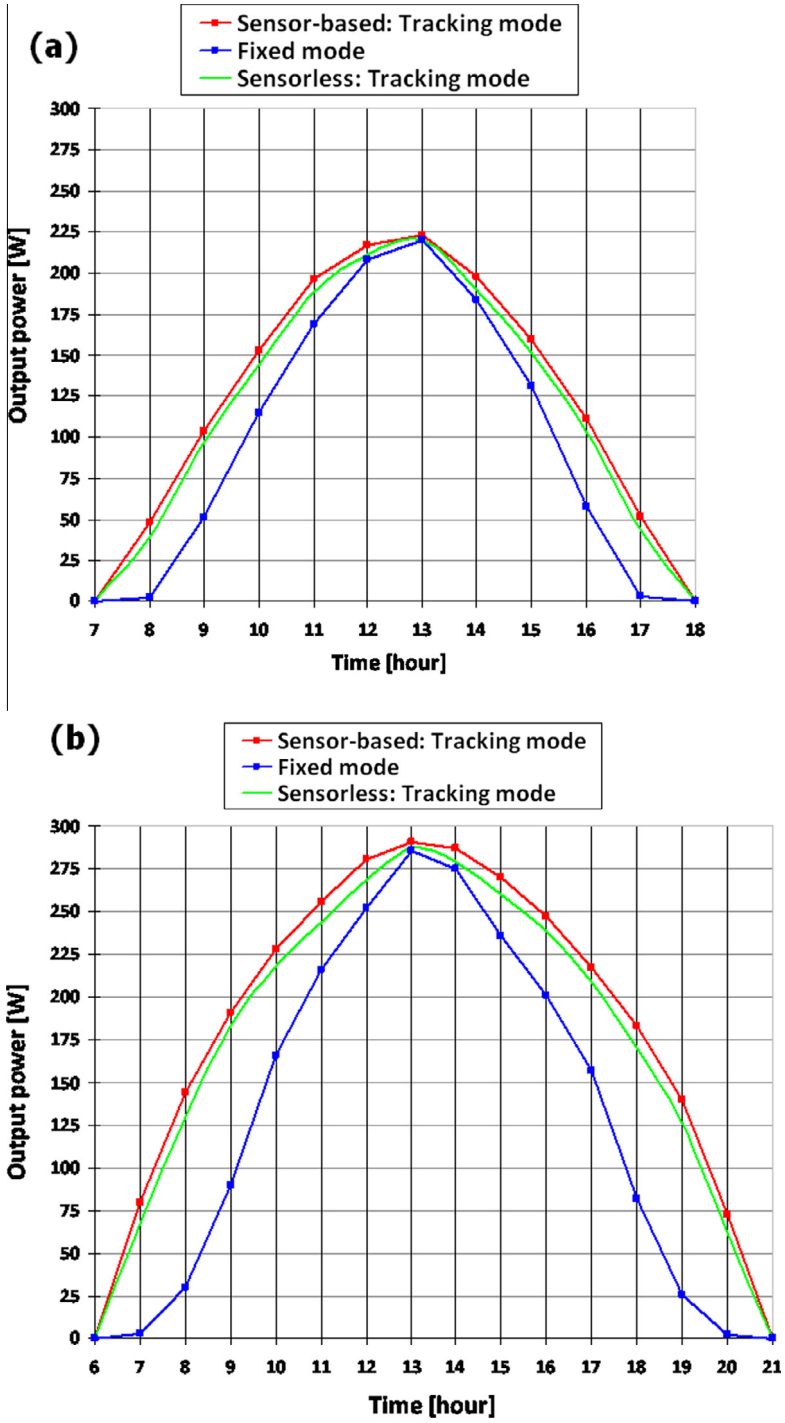

Fig. 8. Comparing between the daily output powers of the PV module on the sensorless and sensor based tracking modes, and fixed mode: (a) On January 19, 2014 in winter and (b) On August 19, 2015 in summer.

sensorless tracking modes are respectively about 2.0220 kW h and 2.6321 kW h in summer, so there is an increase of 30.2% on the sensorless tracking mode. The above-mentioned daily energy measurements and the other measurements related to spring and autumn are summarized in Table 2.

3. Proposed sensor based solar tracker: Implementation and experimental results

The structure of the PV system constructed to implement the proposed sensor based solar tracker is shown in detail in Fig. 9. It consists of the same components used in the sensorless solar tracker, the only difference is the irradiance sensor equipped with the radiance limiting tube which is shown in Fig. 10. It is carried and oriented by an independent dual-axis mechanical system controlled by the microcontroller. The two dual-axis mechanical carriers associated with the sensor and PV module have the identical reference coordinate axes defined for the two systems with reference to the local horizon surface and north (N) direction. The microcontroller gradually varies the altitude and azimuth angles of the sensor, and senses the solar irradiance absorbed by the sensor through pins 19–20. When the solar irradiance peaks, the

Table 2
Average daily electric energy produced by the PV module in four days of four seasons, and increase in the energy efficiency resulted from utilizing the two proposed solar trackers (tracking mode).

Time	Average daily electric energy produced by the PV module [kW h]			Increase in energy efficiency (%)	
	Fixed mode	Sensorless tracking mode	Sensor based tracking mode	Sensorless tracking mode	Sensor based tracking mode
Spring	1.5764	1.9295	2.0887	22.4	32.5
Summer	2.0220	2.6321	2.8844	30.2	42.7
Autumn	1.7314	2.1833	2.3772	26.1	37.3
Winter	1.1422	1.3599	1.4583	19.1	27.7
One year	1.6180	2.0159	2.1879	24.59	35.22

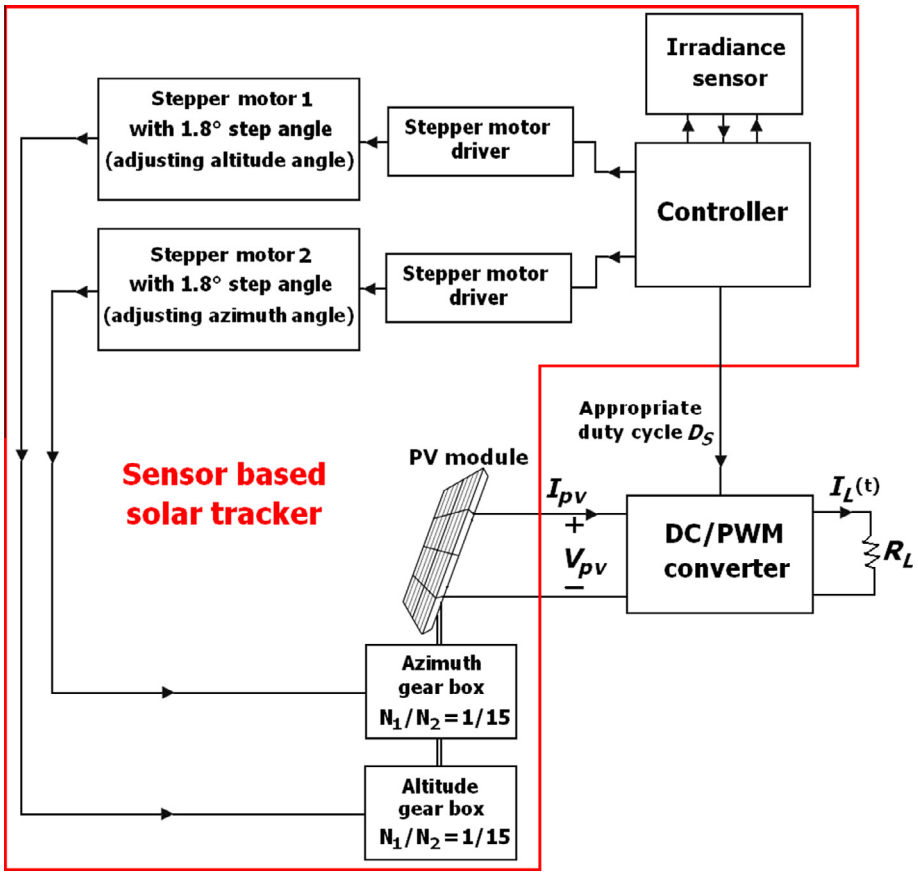

Fig. 9. Structure of the PV system constructed to implement the proposed sensor based solar tracker.

altitude and azimuth angles associated with the instant position of the sensor supplied through pins 17–18 is recorded by the microcontroller as the correct altitude and azimuth angles that should be used to orient the PV module face. Then, similar to what mentioned for the sensorless solar tracker, the microcontroller produces the ten control signals (DIR, NXT, DI, CS, and CLK signals of the two stepper motor drivers) to be supplied to the two stepper motor drivers to rotate the two stepper motors in correct directions with appropriate rotation angles, so that the PV module face is positioned in the sun direction. The electrical circuit of the PV system constructed to implement the proposed sensor based solar tracker is shown in Fig. 11. The circuit operates similar to the sensorless solar tracker explained in detail in Section 2.2, the only deference is that the actual altitude and azimuth angles of the sun position in the sky are determined by the irradiance sensor, and then are delivered to the microcontroller MC68HC11A8 through the two analog to digital conversion (ADC) pins (pins 17–18) of the microcontroller. Based on these two values, the microcontroller produces the ten control signals to be delivered to the two stepper motor drivers to rotate the two stepper motors in correct directions with appropriate rotation angles.

Fig. 7(a) and (b) also compare the actual values of the altitude and azimuth angles of the sun position to the altitude and azimuth angles tracked by the proposed sensor based solar tracker. The comparison shows that the maximum value of the tracking error is 0.14°, and so the tracking error of the proposed sensor based solar tracker is 0.14°. Fig. 8(a) and (b) also compare the daily output powers obtained by the sensor based solar tracker (sensor based tracking mode) to the sensorless tracking and fixed modes in winter and summer. It can be seen from Fig. 8(a) that in winter, the daily electric energies produced by the PV module on the fixed and sensor based tracking modes are respectively about 1.1422 kW h and 1.4583 kW h, and thus, the solar energy converted on the sensor based tracking mode is 27.7% more than that on the fixed mode. Similarly, Fig. 8(b) shows that the daily electric energies obtained on the fixed and sensor based tracking modes

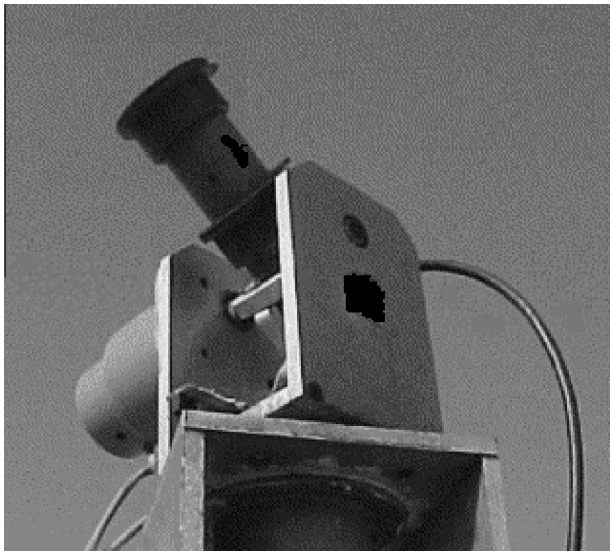

Fig. 10. Irradiance sensor equipped with a radiance limiting tube, and mounted on an independent dual-axis mechanical system.

are respectively about 2.0220 kW h and 2.8844 kW h in summer, so there is an increase of 42.7% in the energy obtained on the sensor based tracking mode. The above-mentioned measurements and the other daily energy measurements related to spring and autumn are also summarized in Table 2.

4. Comparing the two solar trackers to each other and the state-of-the-art trackers

In this section, the two solar trackers are compared from both performance and cost viewpoints, and the results are summarized. Real experimental results obtained in previous sections, and summarized in Table 2 verify that utilizing the sensor based solar tracker increases the average daily solar energy converted to electric power about 27.7%, 32.5%, 37.3%, 42.7% and 35.22% respectively in winter, spring, autumn, summer and during one year while these factors are respectively 19.1%, 22.4%, 26.1%, 30.2% and 24.59% for the sensorless solar tracker. Thus, the sensor based solar tracker causes more increase in solar energy conversion compared to the sensorless solar tracker.

As shown in Fig. 2, the proposed sensorless solar tracker is implemented by adding only two stepper motors, two stepper motor drivers, and two gear boxes to the conventional system. In the constructed system shown in Fig. 6, the prices of the added components are $80 (two stepper motors NEMA 23), $40 (two stepper motor drivers AMIS-30543), and $70 (two gear boxes), and so the total price is about $190. Fig. 9 shows that the sensor based solar tracker includes an extra unit compared to the sensorless solar tracker that is the irradiance sensor equipped with a radiance limiting tube, and mounted on an independent dual-axis mechanical system as shown in Fig. 10. The construction cost of this extra unit is about $265, and so the total price of the sensor based solar tracker is about $455. It is clear that the sensor based solar tracker is also more complicated to be implemented because it needs two independent dual-axis mechanical systems; one for

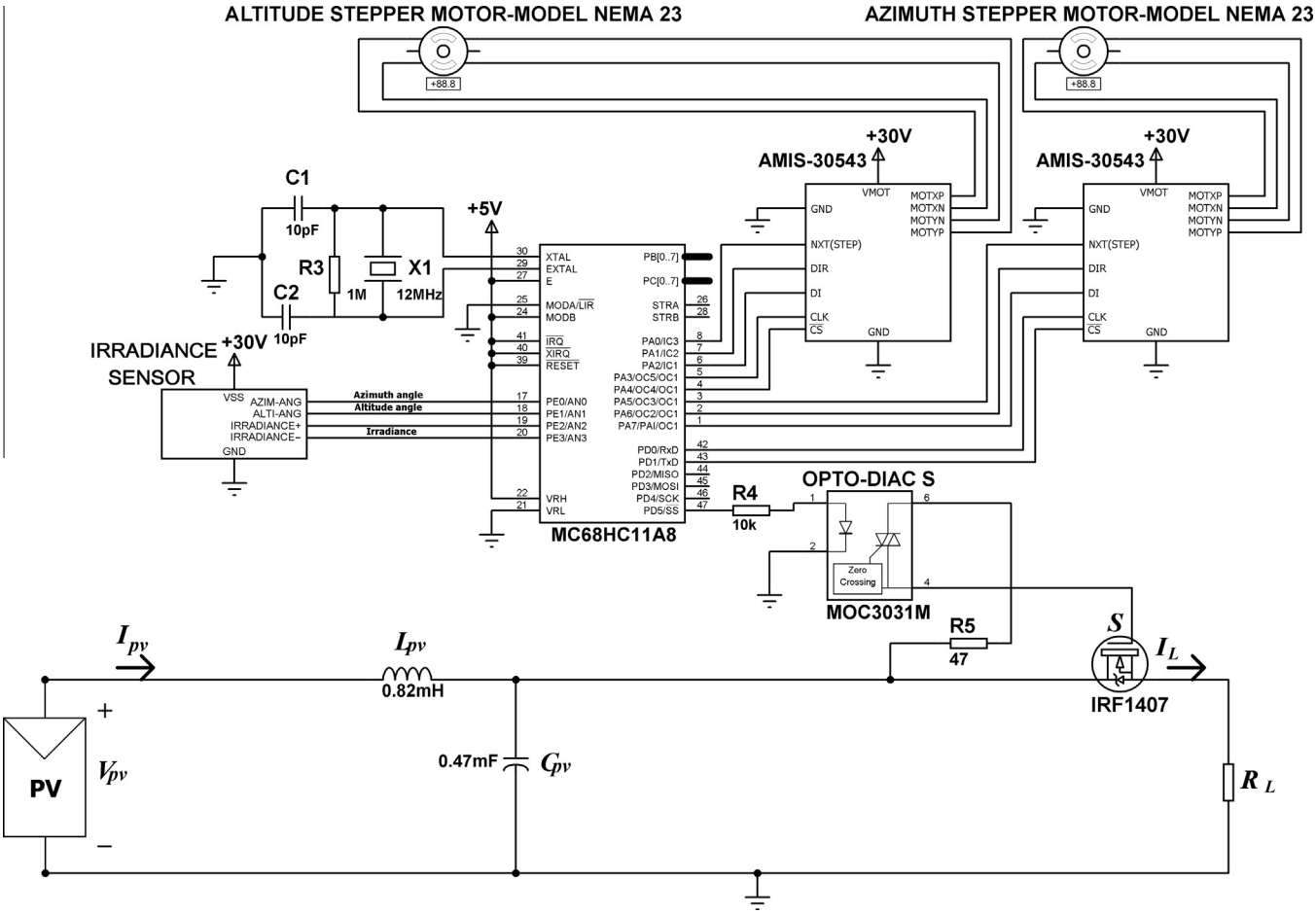

Fig. 11. Electrical circuit of the constructed PV system including the proposed sensor based solar tracker.

Table 3
Comparing the two proposed sensor based and sensorless trackers to each other.

Dual-axis solar tracker type	Complication	Cost ($)	Accuracy	Tracking error	Sensor used in tracker	Number of dual-axis mechanical systems used
Sensor based	High	455	High	0.14°	Yes	2
Sensorless	Low	190	Medium	0.43°	No	1

Table 4
Comparing the two proposed solar trackers to the state-of-the-art solar trackers.

Dual-axis solar tracker type	Sensor based Cañadaa et al. (2007)	Sensor based Wang and Lu (2013)	Sensor based Barsoum (2011)	Sensorless Duarte et al. (2011)	Sensorless Tirmikci and Yavuz (2015)	Sensorless [This work]	Sensor based [This work]
Tracking error	2°	>1°	>1°	>1°	>1°	0.43°	0.14°
Fabrication cost compared to sensorless tracker (this work)	More	More	More	Same	Same	–	More

carrying the sensors, and another for PV module. On the other hand, experimental results presented in Sections 2 and 3 verified that the tracking error of the sensor based tracker is 0.14° while it is 0.43° for the sensorless type. The two solar trackers are compared from different viewpoints in Table 3. It is deduced from Tables 2 and 3 that utilizing the sensor based dual-axis solar tracker will be useful when more energy efficiency is needed. But, if system cost and simplification are more important, the sensorless dual-axis solar tracker can be a good choice. Table 4 compares the two proposed solar trackers to the dual-axis solar trackers reported in the literature in which the tracking error either has been reported or can be estimated. The comparison explicitly shows that the two trackers presented in this work have better performances, i.e., less tracking errors and reasonable costs.

5. Conclusion

In this study, two novel dual-axis solar trackers were designed and constructed, the first one was a sensorless version with the tracking error of only 0.43°, and the second one was a sensor based type with the tracking error of 0.14°. It was shown that these tracking errors are less than that of the state-of-the-art solar trackers. On the one hand, it was demonstrated that utilizing the sensor based solar tracker increases the average daily captured solar energy about 27.7%, 32.5%, 37.3%, 42.7% and 35.22% respectively in winter, spring, autumn, summer and during one year compared to a fixed PV module. These factors are respectively 19.1%, 22.4%, 26.1%, 30.2% and 24.59% for the sensorless solar tracker that are less than that of the sensor based tracker. It is also clear that in a cloudy sky, the sensorless tracker tracks the sun direction in the sky but the sensor based version tracks the direction in the sky that maximum solar irradiance is absorbed by the PV module, and this a benefit of the sensor based tracker. On the other hand, it was verified that the sensor based version is more complicated and expensive than the sensorless tracker. Thus, it is concluded that utilizing the sensor based dual-axis solar tracker will be useful when getting more energy efficiency is the main goal, otherwise the sensorless dual-axis solar tracker will be a good choice when manufacturing cost is more important.

References

Al-Mohammad, A., 2004. Efficiency improvement of photovoltaic panels using a sun tracking system. Appl. Energy 79 (3), 345–354.

Barker, L., Neber, M., Lee, H., 2013. Design of a low-profile two-axis solar tracker. Sol. Energy 97, 569–576.

Barsoum, N., 2011. Fabrication of dual-axis solar tracking controller project. Intell. Contr. Automat. 2, 57–68.

Cañadaa, J., Utrillasb, M.P., Martinez-Lozanob, J.A., Pedrósb, R., Gómez-Amob, J.L., Maja, A., 2007. Design of a sun tracker for the automatic measurement of spectral irradiance and construction of an irradiance database in the 330–1100 nm range. Renewable Energy 32 (12), 2053–2068.

Chin, C.S., 2012. Model-based simulation of an intelligent microprocessor-based standalone solar tracking system. Ebook: MATLAB – A Fundamental Tool for Scientific Computing and Engineering Applications, InTech 3, 251–278.

Chin, C.S., Babu, A., McBride, W., 2011. Design, modeling and testing of a standalone single axis active solar tracker using MATLAB/Simulink. Renewable Energy 36 (11), 3075–3090.

Chong, K.K., Wong, C.W., 2009. General formula for on-axis sun-tracking system and its application in improving tracking accuracy of solar collector. Sol. Energy 83 (3), 298–305.

Duarte, F., Gaspar, P.D., Goncalves, L.C., 2011. Two axes solar tracker based on solar maps controlled by a low-power microcontroller. J. Energy Power Eng. 5 (7), 671–676.

Duffie, J.A., Beckman, W.A., 2013. Solar Engineering of Thermal Processes. Wiley. ISBN: 978-0-470-87366-3.

Eke, R., Senturk, A., 2012. Performance comparison of a double-axis sun tracking versus fixed PV system. Sol. Energy 86 (9), 2665–2672.

Eldin, S.A.S., Abd-Elhady, M.S., Kandil, H.A., 2015. Feasibility of solar tracking systems for PV panels in hot and cold regions. Renewable Energy 85, 228–233.

Fathabadi, H., 2016. Novel fast dynamic MPPT (maximum power point tracking) technique with the capability of very high accurate power tracking. Energy 94, 466–475.

Nenciu, F., Vaireanu, D.-I., 2014. A comparative study for assessing the effectiveness of solar trackers used in conjunction with photovoltaic power autonomous systems. J. Optoelectron. Adv. Mater. 16 (1–2), 102–109.

Quesada, G., Guillon, L., Rousse, D.R., Mehrtash, M., Dutil, Y., Paradis, P.L., 2015. Tracking strategy for photovoltaic solar systems in high latitudes. Energy Convers. Manage. 103, 147–156.

Reda, I., Andreas, A., 2004. Solar position algorithm for solar radiation applications. Sol. Energy 76 (5), 577–589.

Roth, P., Georgiev, A., Boudinov, H., 2005. Cheap two axis sun following device. Energy Convers. Manage. 46 (7–8), 1179–1192.

Sallaberry, F., Pujol-Nadal, R., Larcher, M., Rittmann-Frank, M.H., 2015. Direct tracking error characterization on a single-axis solar tracker. Energy Convers. Manage. 105, 1281–1290.

Syafii, Nazir, R., Kamshory, Hadi, M., 2015. Improve dual axis solar tracker algorithm based on sunrise and sunset position. J. Electr. Syst. 11 (4), 397–406.

Tina, G.M., Gagliano, S., Graditi, G., Merola, A., 2012. Experimental validation of a probabilistic model for estimating the double axis PV tracking energy production. Appl. Energy 97, 990–998.

Tirmikci, C.A., Yavuz, C., 2015. Comparison of solar trackers and application of a sensor less dual axis solar tracker. J. Energy Power Eng. 9, 556–561.

Wang, J.M., Lu, C.L., 2013. Design and implementation of a sun tracker with a dual-axis single motor for an optical sensor-based photovoltaic system. Sensors 13 (3), 3157–3168.

Wu, J., Chen, X., Wang, L., 2016. Design and dynamics of a novel solar tracker with parallel mechanism. IEEE/ASME Trans. Mechatron. 21 (1), 88–97.

Yao, Y., Hu, Y., Gao, S., Yang, G., Du, J., 2014. A multipurpose dual-axis solar tracker with two tracking strategies. Renewable Energy 72, 88–98.

Zhang, P., Zhou, G., Zhu, Z., Li, W., Cai, Z., 2013. Numerical study on the properties of an active sun tracker for solar streetlight. Mechatronics 23 (8), 1215–1222.